Department of Electrical and Computer Systems Engineering

Technical Report
MECSE-18-2003

LiNbO3 broandband Interferometric optical modulators; modelling and implementation

L.N. Binh and T.W. Chua

MONASH UNIVERSITY

LiNbO₃ broadband interferometric optical modulators: modelling and implementation

L.N. Binh, A. Le and T.W. Chua

Laboratory for Optical Communications and Applied Photonics, Department of Electrical and

Computer Systems Engineering, Monash University, P.O. Box 35, Clayton, Victoria 3800,

Australia

ABSTRACT

An accurate and yet simple simulation technique for optical modulators operating at multi-GHz region and optical modulators are critical for Tera-bps optical communications. This paper describes a simple, efficient and accurate analysis of the travelling wave electrodes for high pseed optical modulation and the implementation of these electrodes in interferometric optical modulators.

A finite difference approach is employed in modelling the traveking wave eletrodes for efficient electro-optic interaction in interferometric optical modlators. Eletrode configurations such as symmetric and asymmetric co-planar waveguide or strip structures and shielded electrode systems can be modelled. Simulated results demonstrate the efficiency of the presented method as compared with other methods such as the Green's function, conformal mapping, method if images, spectral domain analysis etc. Tilted and thick practical eletro-plated electrodes are modeled and confirmed with implemented modulators operating up to 26 GHz in diffused LiNbO₃ optical interferometric

optical waveguide structures. The fabrication of optical waveguides and travelling wave electrodes are described for implemenation of the electro-optic interferometric modulators.

Keywords: optical modulators, finite difference techniques, optical communications, optical waveguides

1   INTRODUCTION

Optical communication systems have now reached an increasing fast pace in both speed and capacity with OC-192 then OC-768 and beyond, eg. optical transmitters for 80 Gbps and 160 Gbps in the near future. External modulation is the most important technique for modulating lightwaves greater than 10 Gbps. Electrooptic modulators in $LiNbO_3$ waveguiding structures has been contributing significantly in the last two decades in the technological evolution of optical fibre communications due to its intrinsic high-speed property. Further the modulation format of carrier suppressed return-to-zero (CS-RZ) consisting of two interfrometric modulators in tandem demands an efficient and accurate modelling of the travelling wave electrodes and the interaction of the launched travelling waves in such combined electro-optic modulation system.

This paper thus dedicates to detailed modelling of the interferometric optical modulators incorporating travelling wave electriodes and optical interferometric waveguiding sstructures together with their implementation in LiNbO3 system.

The design of travelling wave elevctrodes are based on adopted empirical model derived from the combination of the quasi-TEM analysis and the Green function method. The empirical model, despite being impressive in its ability to facilitate the design calculation, does not provide the

modulating electric field that is mandatory in calculating the electro-optical overlap integral. More importantly, it does not take into account of the more subtle structural factors such as the wall angle of the gold plated electrode[21]. Most analyses such as the conformal mapping technique[1], the Green function method[4-5] or the method of images[3,15], either assumes an infinitely thin electrodes or assume the wall angle of the electrode to be 90°. However when very thick electrodes, typically in the range of 10 to 20 μm[20,21], are employed to achieve broadband operation capable of handling bandwidth of more than 40 GHz, the 90° wall angle assumption is no longer valid. In practical devices, after electro-plating process, the electrode normally assumes a trapezoidal shape as shown in Figure 1(b). Figure 1(a) shows the schematic plane view of the electro-optic interfferometric optoical modulators. The wall angle of the electrode in fact has a rather significant influence on the value of effective microwave index n_m and characteristic impedance Z. It is therefore important to take into considerations such structural effect of the electrodes in the design of travelling wave electrodes. Chung *et al.*[4,5] modelled the electric field of the electrodes with the Green function method. Unfortunately their analysis has not taken intoconsideration of the effect of the wall angle that is a common feature in the fabrication of travelling wave eletrode by eletro-plating. Such electrode structural factors can only be modelled by a more robust numerical formulation such as the finite element method[12-13, 19-20] or the finite difference method[18]. We employ the finite difference method for solving the anisotropic Laplace equation due to its relatively simple but sufficiently accurate analysis.

This paper is organised as follows. In the next section we outline the numerical formulation of non-uniform meshed finite difference scheme to solve the anisotropic Laplace equation under a quasi-TEM assumption of the microwave mode. Based on this numerical model, the analytical system, the

Finite Difference Travelling Wave Electrodes Analysis (FDTWEA), is developed to model the electrode parameters Z and n_m, the optical modulated fields, E_x and E_y, and the travelling wave – optical waves interaction overlap integral, Γ representing the efficiency of the modulation of lightwaves in an interferometric optical system. Comparisions of our calculations with published results to verify the validity, the simplicity and efficiency of FDTWEA are given. A study of the effect of the wall angle on electrode design is described. The analysed electrodes are in-corporated in interferometric optical waveguiding systems for optimisation of the performance of optical modulators. Implementation of the interferometric modulators operating up to 30 GHz is described.

2   ELECTRODE MODELS AND ELECTRO-OPTIC INTERFEROMETRIC MODULATION

2.1   Finite difference models for RF travelling wave electrodes

Travelling wave electrodes are miniature transmission lines where quasi-TEM wave propagation can be assumed. The electric field can thus be approximated by a two-dimensional electrostatic field problem that can be solved by the well-known Laplace equation. A Z-cut LiNbO$_3$ crystal is used for the analysis and later in experiments presented herewith. Other substarte orientations such as the X- and Y-cut can be adapted without difficulty by considering the tensor properties of the electro-optic interaction. The permittivity tensor matrix is diagonal[1] and the electrostatic potential V is essentially the solution of the anisotropic Laplace equation given as

$$\frac{\partial}{\partial x}\left(\varepsilon_x \frac{\partial V}{\partial x}\right) + \frac{\partial}{\partial y}\left(\varepsilon_y \frac{\partial V}{\partial y}\right) = 0$$

(1)

A non-uniform mesh allocation scheme is used to economise computer memory requirement. Denser mesh is allocated at the edges of the electrode and also the buffer layer area so that the effect of the edge field can be modelled more accurately. On the other hand nodes located further away from the electrode can be modelled with a coarser mesh. The steps involved in formulating the difference equation[19] can be briefly outlined. Considering a general electrode structure as shown in Figure 2 with grid points placed along dielectric boundary, the electrode structures involve only three dielectric media, namely, the air, the SiO_2 layer and the $LiNbO_3$ substrate. The boundary conditions can be considered for nodes positioned along the boundary, say P and four other points surrounding it, namely, A, B, C and D. The mid-points between AP, BP, CP and DP are labelled in order of 1, 2, 3 and 4 and their respective grid sizes are denoted as h_a, h_b, h_c and h_d. The corresponding electrical field potentials are V_P, V_A, V_B, V_C and V_D, respectively. K_{e1} and K_{e2} are the dielectric constants of the medium.

$$At\ point\ 1,\ \frac{\partial V}{\partial x} \approx \frac{V_P - V_A}{h_a} \quad (2a); \qquad at\ point\ 2, \quad \frac{\partial V}{\partial x} \approx \frac{V_B - V_P}{h_b} \quad (2b);$$

$$at\ point\ 3,\ \frac{\partial V}{\partial y} \approx \frac{V_C - V_P}{h_c} \quad (2c); \qquad and\ finally\ at\ point\ 4,\ \frac{\partial V}{\partial y} \approx \frac{V_P - V_D}{h_d} \quad (2d)$$

With the assumption that half of the flux flows in medium 1 and the other half flows in medium 2, we have

$$\left(\varepsilon_x \frac{\partial V}{\partial x}\right)_{PB} = \frac{\frac{1}{2}(Ke_{1x} + Ke_{2x}) \cdot (V_B - V_P)}{h_b} \quad along\ segment\ PB\ (3a); \quad \left(\varepsilon_x \frac{\partial V}{\partial x}\right)_{AP} = \frac{\frac{1}{2}(Ke_{1x} + Ke_{2x}) \cdot (V_P - V_A)}{h_a} \quad for\ AP$$

(3b)

$$\left(\varepsilon_y \frac{\partial V}{\partial y}\right)_{PC} = \frac{Ke_{2y} \cdot (V_C - V_P)}{h_c} \qquad \text{along PC (3c)}; \qquad \left(\varepsilon_y \frac{\partial V}{\partial y}\right)_{DP} = \frac{Ke_{1y} \cdot (V_P - V_D)}{h_d} \qquad \text{along}$$

DP *(3d)*

Thus the Lapace equation (1) becomes

$$\frac{\left(\varepsilon_x \frac{\partial V}{\partial x}\right)_{PB} - \left(\varepsilon_x \frac{\partial V}{\partial x}\right)_{AP}}{\frac{1}{2}(h_a + h_b)} + \frac{\left(\varepsilon_y \frac{\partial V}{\partial y}\right)_{PC} - \left(\varepsilon_y \frac{\partial V}{\partial y}\right)_{DP}}{\frac{1}{2}(h_c + h_d)} = 0$$

(4)

Hence by substituting (3) into (4), a five-point difference equation can be derived as

$$K_A V_A + K_B V_B + K_C V_C + K_D V_D - K_P V_P = 0 \qquad (5)$$

where $K_A = \dfrac{Ke_{1x} + Ke_{2x}}{hb \cdot (ha + hb)}$ *(6a)*; $\qquad K_B = \dfrac{Ke_{1x} + Ke_{2x}}{ha \cdot (ha + hb)}$ *(6b)* ; $K_C = \dfrac{Ke_{2y}}{\frac{1}{2}hc \cdot (hc + hd)}$ *(6c)*;

$K_D = \dfrac{Ke_{1y}}{\frac{1}{2}hd \cdot (hc + hd)}$ *(6d)*; $\qquad$ and $K_P = K_A + K_B + K_C + K_D$ *(6e)*

Considering the schematic diagram as shown in Figures 1 and 2, the boundary conditions can be formulated. At the interface between air and the SiO$_2$ buffer layer, there exists the homogeneous medium where $Ke_{1x} = Ke_{2x} = Ke_{1y} = Ke_{2y}$. So we have

$K_A = \dfrac{1}{h_a \cdot (h_a + h_b)}$ *(7a)* ; $\quad K_B = \dfrac{1}{h_b \cdot (h_a + h_b)}$ *(7b)* ; $K_C = \dfrac{1}{h_c \cdot (h_c + h_d)}$ *(7c)*; and

$K_D = \dfrac{1}{h_d \cdot (h_c + h_d)}$ *(7d)*

Along the buffer and crystal boundary, $Ke_{1x} = Ke_{1y} = \varepsilon_b$, $Ke_{2x} = \varepsilon_x$, $Ke_{2y} = \varepsilon_y$,

therefore

$$K_A = \frac{\varepsilon_b + \varepsilon_x}{h_a \cdot (h_a + h_b)} \ (8a) \ ; \quad K_B = \frac{\varepsilon_b + \varepsilon_x}{h_b \cdot (h_a + h_b)} \ (8b); \quad K_C = \frac{2\varepsilon_y}{h_c \cdot (h_c + h_d)} \ (8c); \ and \quad K_D = \frac{2\varepsilon_b}{h_d \cdot (h_c + h_d)}$$

(8d)

In the guiding region and the substrate LiNbO₃, $Ke_{1x} = Ke_{1y} = \varepsilon_b$, $Ke_{2x} = \varepsilon_x$, $Ke_{2y} = \varepsilon_y$, *therefore*

$$K_A = \frac{2\varepsilon_x}{h_a \cdot (h_a + h_b)} \ (9a); \quad K_B = \frac{2\varepsilon_x}{h_b \cdot (h_a + h_b)} \ (9b); \quad K_C = \frac{2\varepsilon_y}{h_c \cdot (h_c + h_d)} \ (9c); \quad and \quad K_D = \frac{2\varepsilon_y}{h_d \cdot (h_c + h_d)}$$

(9d)

For nodes located in the electrodes, we have $K_A = K_B = K_C = K_D = 0$, $K_P = 1$. Using a sufficiently large space of approximately 400×400 μm, the electric field along the window boundary to be zero can be assumed to zero. For the potential, it is essentially that Neumann boundary conditions[19, 30] can be established as

For upper window boundary $K_A V_A + K_B V_B + 2K_C V_C - K_P V_P = 0$ *(10); for left hand window*

boundary $2K_B V_B + K_C V_C + K_D V_D - K_P V_P = 0$ *(11); and for top left hand corner*

$2K_B V_B + 2K_C V_C - K_P V_P = 0$ *(12)*

The rest of the windows are just the permutation of the boundary conditions as described. Incorporating the boundary conditions into the difference equations, we obtain a set of difference equations derived from each grid point resulting in an eigen-matrix equation

$$\mathbf{A}.\mathbf{u}=\mathbf{b} \tag{13}$$

where **A** is the coefficient matrix, **u** is the vector representing the potential at grid points, while **b** is the vector that assumes the RHS of.(1) which is mostly null except for the grid points on the electrodes assuming the values of the potential in the electrode regions. Figure 2(a) shows the grid size and the formation of the matrix coefficients. The difference matrix equation can be solved by conventional successive overelaxation method[19,30]. This method, however, requires a good initial guess and a good estimate of the relaxation factor in order to have a reasonable rate of convergence. Using ITPACK NSPCG[31], the eigenvalue matrix can be solved relatively quickly with high accuracy. ITPACK matrix solver applies various accelerators and preconditioners in solving the matrix. For a banded matrix, there needs to store only the nonzero elements inorder to significantly economise the computer memory usage. The Othormin (Omin) accelerator and incomplete Cholesky preconditioner can be used[31] and the solution of the anisotropic Laplace equation enable calculations of various properties of the microwave RF electrodes.

2.2   Travelling wave electrodes: line capacitance, characteristic impedance and microwave effective index

The whole purpose of carrying out the above numerical formulation is eventually to compute the relevant travelling wave electrodes parameters such as the characteristic impedance Z and the microwave effective index n_m given by

$$Z = \frac{1}{c\sqrt{CC_o}} \qquad (15) \qquad and \ the \ microwave \ effective \ index \ n_m \ defined \ as \quad n_m = \sqrt{\frac{C_o}{C}}$$

$$(16)$$

where C is the capacitance per unit length of the transmission line with the dielectric medium, while C_0 is the capacitance per unit length for the air filled medium, with c being the speed of light in vacuum. To compute these quantities the line capacitance C and C_0 of the transmission line in the dielectric medium and air, respectively must be determined. To obtain the capacitance it is prerequisite to determine the charges on the conductors which may be found by applying Gauss's theorem[26], which requires integration of the normal component of the electric flux over a surface enclosing the hot electrode as shown in Figure 2(c). Forming this surface by lines joining the nodal points drawn parallel to the coordinate directions at any point P on this surface, we have

$$D_n = \varepsilon E_n = -\varepsilon \frac{\partial V}{\partial n} \tag{17}$$

where D_n is the normal component of the electric flux, E_n is the normal component of electric intensity, and n is the normal coordinate, which for a square box would be x, and y. The potential at P may be expressed in terms of the known potentials V_A and V_b on each side of it. For irregular mesh shown in Figure 2(b) we have

$$\frac{\partial V}{\partial x} = \frac{V_B - V_A}{h_b + h_a} \tag{18}$$ and $$\frac{\partial V}{\partial y} = \frac{V_C - V_D}{h_c + h_d} \tag{19}$$

Applying Gauss' theorem for a closed surface of an arbitrary shape containing the hot conductor of s straight line segments each containing r, the charge per unit length normal to the cross section would then be given by

$$Q = \varepsilon_r \varepsilon_o l \sum_s \sum_{P=1}^{4} {}' \left(\frac{\partial V}{\partial n} \right)_P \tag{20}$$

where the apostrophe sign is used to indicate that the first and last terms in the summation are halved, that is seen to be equivalent to integration by the trapezoidal rule, l is the length of the infinitesimal segment of the integration path. For uniform discretisation, l is essentially the grid size h. For non-uniform grids, l is assumed to be either $(h_a+h_b)/2$ or $(h_c+h_d)/2$ depending on either a horizontal or vertical line segment over which the summation is taken. The relative permittivity, ε_r depends on the dielectric medium on which the point P is located. For example, a summation of the derivative along the first horizontal segment ($s=1$) where it lies completely in the air, then $\varepsilon_r=1.0$. Similarly for segment 3 which is in the LiNbO$_3$ crystal and $\varepsilon_r= \varepsilon_z=43$. The vertical summation ($s=2$, 4), however, needs to be taken with care because it is in the transitional region between two dielectric media. For points which are entirely in the air, SiO$_2$ and LiNbO$_3$, the relative permittivities are $\varepsilon_a =1.0$, $\varepsilon_b=3.9$ and $\varepsilon_x=28$, respectively. However, for points that fall on the buffer air interface, we assume half of the flux pass through each medium. So for air-SiO$_2$ interface, $\varepsilon_r=(1+ \varepsilon_b)/2$. Whereas for the SiO$_2$-LiNbO$_3$ interface, $\varepsilon_r=(\varepsilon_b+ \varepsilon_x)/2$. Using the charge capacity given by C = Q/V$_t$ with V_t the potential difference between the conductors assumed be unity to simply our calculation, C_o, can be obtained by solving the Laplace Equation for the transmission line in the air filled medium without the dielectric and go through similar process to work out the charge capacity and hence the capacitance. Once both C_o and C are determined, both the characteristic impedance, Z and microwave effective index, n_m can be determined by (15) and (16).

2.3   Electro-opticmodulation overlap integraland small signal frequency response

The electric fields of the travelling waves in the x and y directions can be determined from the electric potentials at grid locations as

$$E_x = \frac{\partial V}{\partial x} = \frac{V_B - V_A}{(h_a + h_b)} \qquad (21) \quad and \qquad E_y = \frac{\partial V}{\partial y} = \frac{V_C - V_D}{(h_c + h_d)} \qquad (22)$$

The electro-optic interaction of the modulator can be detrimned via the overlap integral, Γ given by[15,16]

$$\Gamma = \frac{g}{V} \iint |E_o(x,y)|^2 E_m(x,y)\,dxdy \qquad (23)$$

where $|E_o(x,y)|^2$ is the optical filed intensity distribution of the optical guided waves and E_m is the electrical field of the electrodes. The choice of E_x or E_y depends on the crystal orientation and the polarisation of the optical field. We can indeed assume that the normalised optical field intensity profile assumes a Hermition Gaussian profile that is defined as[15,16]

$$|E_o(x,y)|^2 = \frac{4y^2}{w_x w_y^3 \pi} \exp\left[-\left(\frac{x-p}{w_x}\right)^2\right] \cdot \exp\left[-\left(\frac{y}{w_y}\right)^2\right] \qquad (24)$$

where the 1/e intensity width and depth are $2w_x$ and $1.376w_y$, respectively, and p is the peak position of the optical field in the lateral direction. w_x and w_y are dependant on the fabrication parameters of the optical waveguide and can either be determined experimentally or by the optical waveguide mode modelling. We experimentally determine the optical fields by measuring these optical mode fields of optical waveguides fabricated by in-diffusion of the titanium strips into LiNbO3.

The small signal bandwidth is effectively the most critical factor in the high frequency operation of the interferometric modulators. An applied RF voltage as seen at any point along the electrode by a lightwave that enters the waveguide at a time t_o can then be written as

$$V(z, to) = V_0 \sin(\frac{2\pi n_m f}{c}(1 - \frac{n_o}{n_m})z - 2\pi f_o t) \qquad (25)$$

where n_o is the effective refractive index of the guided optical mode. For the interferometric modulators, the optical modulation is determined by the total induced phase shift introduced along the interaction length, L. The walk-off results in a frequency-dependent reduction in the integrated phase shift, which can be obtained by integrating the voltage that affects the light over the electrode length and given by

$$\frac{\int_0^L \Delta\beta(f)dz}{\overline{\Delta\beta}} = \frac{\sin(\pi T f)}{\pi T f}\sin[\pi(2t_o - T)f] \quad (27) \quad \text{where} \quad \overline{\Delta\beta} = \frac{\pi n_e r_{33} L}{\lambda}\frac{V_o}{g}\Gamma \qquad (26)$$

in which n_e and r_{33} are the extraordinary index and electrooptic coefficient of LiNbO3, respectively, l is the optical wavelength, g is the inter electrode gap, while $T=L(n_m-n_0)/c$. is the transit time[30,31] resulting from the velocity mismatch between the copropagating optical and microwave signals. For $n_m=n_o,$ the optical wave travels down the waveguide at the same speed as the microwave drive signal travels along the electrode length, and consequently experiencing the same voltage over the entire electrode length. In this case the integrated value of $\Delta\beta$ is proportional to $V_0 L,$ and arbitrarily long electrodes can be used to reduce the required drive voltage with no frequency limitation. Unfortunately, for $n_o \neq n_m$ there is a walk off between the optical wave and microwave drive signal which results in a reduction of available bandwidth, or, for sufficiently large length, L or frequency, f, a complete cancellation of $\Delta\beta$. In other words, in the design and implementation of of electrodes, the microwave index, n_m must be as close as possible to the optical refractive index. This is implemented by electroplating the elkectrode as thick as possible.

The frequency response function of the modulators can be derived by examining the frequency dependant total phase shift that results from applied microwave voltage[4,30]

$$H(f) = e^{-(\alpha L/2)} \left[\frac{\sinh^2\left(\dfrac{\alpha L}{2}\right) + \sin^2\left(\dfrac{\xi L}{2}\right)}{\left(\dfrac{\alpha L}{2}\right)^2 + \left(\dfrac{\xi L}{2}\right)^2} \right] \tag{27}$$

where $\xi = 2\pi f(n_m - n_o)/c$ and α is the attenuation constant due to electrical and dielectric loss usually characterised by the S_{12} parameter of the RF electrode. The bandwidth to be defined is the electrical small signal bandwidth with the device biased in a region where the optical output intensity is approximately a linear function of the applied voltage[30], where V_π is the d.c. voltage required to create a phase difference $\Delta\beta$ of π by $V_\pi = \dfrac{\lambda g}{n_e^3 r_{33} L \Gamma}$. The overlap integral, Γ, can be calculated independently without affecting the impedance Z and effective microwave index n_m in the electrode design. In other words, the maximisation of Γ can be done separately. To have a low V_π, we need to maximise the overlap integral. This can be achieved by careful fabrication of Ti:LiNbO$_3$ waveguide with the tightest confined optical mode. The design and fabrication process of Ti:LiNbO$_3$ waveguide has already been outlined. In our preliminary design calculation, the value of Γ is specified as an independent parameter to calculate V_π.

The bandwidth is 3-dB optical intensity modulation depth. For systems where the originating and received signals are ultimately electrical, the electrical bandwidth is more relevant. The small signal bandwidthcan be determined by solving (28) for the frequency at which $H(f) = 1/\sqrt{2}$. This can be

achieved by using the bisection search algorithm. For a lossless electrode, $H(f)$ is reduced to sinc($\xi L/2\pi$) and the bandwidth would be approximated by

$$B.W \cong 1.4c / [\pi L(n_m - n_o)] \tag{28}$$

This expression can also be used as a rule of thumb for electrode design and allows us to calculate the required electrode length by specifying the optical bandwidth of the transfer function $H(f)$ and how the difference in optical and microwave index, $\Delta n = n_m - n_o$, the loss constant, α_0 and the electrode length, L can affect the bandwidth of the optical response. The modulator bandwidth can be extended by reducing Δn to its possible minimum value. These parameters can be optimised in the later section.electrode losses, the bandwidth of travelling wave devices depends on the length, velocity mismatch and also the device type, which for our case is an interferometric type device.

3 DESIGN MODELLING AND IMPLEMENTATION

3.1 Electrode structures and performance

Contour plots of the potentials, and thence the electric fields for modulating the optical phase, for CPW, ACPS and CPS electrode structures can be obtained via the solutions of the above-described Laplace equations. The finite difference technique is modeling three structures with the dimensions of w=10 μm, g=15 μm, t=3 μm and t_b=1.2 μm. Once the electric fields E_x, and E_y of the travelling wave electrodes are obtained for each structure, the optical fields profile of the fiundamental lightwave mode are designed for matching, hence broadband operations of the interferometric optical modulators. The E_x component is strongest in region between the gaps while E_y is strongest along the hot electrodes in all travelling type structures. We note also that the push pull operation

can be achieved most efficiently by E_x of a co-planar waveguide (CPW) electrode structure for the X-cut Y-propagating device.

Another structure consisting of optical waveguides positioned directly underneath is the (coplanar strip) CPS electrode by taking full and effective strength of E_y in a Z-cut LiNbO$_3$. The CPS structure, however, suffers high propagation loss[20] and is therefore seldomly used. Another common configuration for Z-cut device is to place one waveguide under the hot electrodes and the other at the edge of the ground plane in either the CPW or (asymmetric coplanar strips) ACPS structure similar to the electrode incorporated in Figure 1. E_y is used in such configuration. This however cannot be considered as a full push-pull operation because the waveguide underneath the electrode ground plane effectivey sees only half of the optical guided placed under the hot electrode. Strongest field exists around the edges of the electrodes, within the SiO$_2$ buffer layer underneath the hot electrodes and also in the gap between the electrodes. It is therefore necessary to assign denser finite difference grids in these regions. For regions further away from the electrodes, a coarser grid size is used. In preliminary simulation a grid size as small as 0.05 μm to 0.2 μm at around the electrode edges is uses, the gap and buffer region, up to larger grid size of 8 to 10 μm for points where the electric field has decayed substantially and accurate results can be obtained. It is found that a problem space of around 400 by 400 μm is sufficient to assume a metal box boundary condition. An average grid size for that problem space would be around 300 by 200 points. With the band storage mode employed by the matrix solver and a work station environment, such dense grid mesh can be supported without any problem. The average amount of time taken to complete a typical simulation would be around 3 to 5 minutes on a DECAlpha3000/300L workstation depending on the load of the computer since we are working in a multi-user system. With this

consumption of computing time current PCs with CPU clock rate of 1 Gb/s and 256 Mbytes RAM can be used to model these electrodes and optical modulation at ease.

3.1.1 Electrode modelling accuracy and comparisons with other techniques

We compare the values of Z and n_m with several published experimental results that are tabulated in Table 1. The calculation of FDTWEA for both the CPW electrodes compares well with the measured results published by Chung et al.[5]. In the modelling the Z and n_m values are obtained for the buffer layer varying from 0.6 to 0.85 because these two values of t_b are determined from the fabrication tolerances of practical devices. Calculated results have agreed very well with measured values of fabricated modulators.

Ref.	Electrode	W(μm)	g(μm)	t(μm)	t_b(μm)	Published		FDTWEA	
						n_m	Z(Ω)	n_m	Z(Ω)
[5]	CPW	20	5	3	0.6-0.85	2.7	27	2.867 - 2.703	25.7- 27.3
	CPW	48	10	3	0.6-0.85	3.3	24.5	3.358 - 3.224	24.13 - 25.14
[22]	ACPS	15	5	4	0	-	~35	3.661	29.83
		15	5	0	0	-	-	4.226	35.315
[16]	ACPS	10	10	1.5	0.1	-	45(Cal),47.1(TDR) 49.8(NA)	3.781	45.27

Table 1: FDTWEA calculated results as compared with published results

There seems to be a discrepancy in our calculated Z value of the ACPS structure compared to that reported in Ref..[22]. However Ref.[22] has not indicated how Z of 35Ω could be obtained. We therefore assumed that in their calculations the thickness of the electrodes was not taken into account. Our recalculation of the impedance in assuming that of an infinitely thin electrode, gives an impedance of 35.315 Ω. This value agrees well with the reported value in [22]. Our modelling is

again confirmed with experimental results reported by Chuang *et al.*[16] and is consistent with calculated results based on the method of image. However, the measured result differs slightly from the theoretical predictions. The characteristic impedance measured by the time domain reflection and by using network analysis techniques were 49.8Ω and 47.1Ω, respectively. A slight discrepancy is possibly due to the effect of slightly thicker SiO_2 buffer layer.

The effective microwave index n_m for very thick electrodes agrees well with those obtained by the finite element method[13] and are shown in Figure 4. The thickness of the electrodes can significantly improve the electrical and optical velocity matching. Thick electrodes that are in the range of 10-20 μm are employed. Calculated results using finite difference approach and those by the finite difference method agree to within 0.5%. A grid size of 0.125 μm along the wall of the thick electrodes is employed in our calculations. The finite difference scheme presented in this paper has achieved similar level of accuracy in a relatively straightforward numerical analysis and efficient use of computing resources. Thus it can be employed for much more complex electrode structures in optical modulation systems such as a composite, cascaded or cascode electrode structures. Our assessment has shown that the finite difference scheme is capable of calculating the travelling wave electrode parameters, namely Z and n_m with high precision. The FDTWEA would therefore be a useful tool to provide a quantitative measure for the design of travelling wave electrodes for integrated electro-optic interferometric intensity and phase modulators in $LiNbO_3$ and/or in semiconductor systems.

3.2   Electro-optic overlap integral factors

In this section, simulated results for the overlap integral between the travelling wave field and the optical guide waves are given. Obviously in order to compute the overlap integral, we need the normalised optical intensity field profile that follows a Hermittion-Gaussian profile as given by (25).   The mode size of the optical field influences the overlap integral Γ, and hence the modulation efficiency of the optical modulator. The variables that characterise the optical guided mode size are w_x and w_y, which are twice the 1/e modal width and 1.376 times the 1/e modal depth. w_x and w_y can either be calculated using standard modelling of optical fields in channel optical waveguides or by experimentally measured mode size. Another important attribute that affects Γ is the relative position of the optical mode with respect to the hot electrodes. All the attributes that affect the value of Γ can be easily modelled by FDTWEA. Γ for the ACPS electrodes and effects of various factors on this overlap integral are given. The ACPS is most preferred in CS-RZ intensity modulators operating around 40 GHz due to its simplicity in launching the RF travelling waves by only one electrode rather than that of the CPS where two in-phase microwaves must be excited.

Figures 5 shows the variations of the overlap integral, Γ as the peak position of the optical mode, p shifts from one end of the electrodes to the other end. The plots indicate quantitatively how the spot size of the optical mode field influence the overlap integral factor Γ. As expected, a tighter confined mode would gives a higher value of Γ. It is therefore important to design and fabricate Ti-diffused LiNbO$_3$ waveguide that can give the smallest possible mode size. Apart from having a tightly confined optical mode, the relative position of the optical waveguide with respect to the electrodes is also extremely important to maximise the contribution of the electro-optic effect.

When narrow electrodes are used with the electrode width comparable to the size of the waveguide, then it is preferred to place the waveguide directly underneath the electrode to utilise the strong edge field from both side of the electrode. This has been shown in Figure 9 where maximum Γ is obtained when the position of the optical mode is centred under the electrode. However, for a much wider electrode width, the preferred position would be just inside the end of the electrode closer to the gap when a 30μm wide electrode is employed. A maximum overlap integral can be achieved by exploiting the higher edge field by centralising the waveguide at x~135 μm.

Having the optical waveguide right at the centre of the electrode would be an inefficient design. Figure 7 shows dependence on the electro-optic interaction by the thicker buffer layer. Although a thicker buffer layer has the advantage of a lower conductor loss and also significantly improves the velocity match, there is a trade off involved because the overlap integral is lower, which can therefore lead to a higher V_π. We can see that without the buffer layer, Γ assumes a much higher value. Unfortunately, having no buffer layer would imply a much higher optical-electrical velocity mismatch.

3.3   Effects of angled-wall structure on RF electrodes

In previous sections, FDTWEA has been used to analyse various rudimentary design parameters of the travelling wave electrodes. This technique has been employed to study other electrode structures of higher degree of complexity. The shielded phase velocity-matching travelling wave electrode structure proposed by Kawano *et al.*[11-12] can be analysed with accuracy. Furthermore the analysis of wall angled electrodes as proposed by Gopal *et al.*[21] is also analysed by our method confirming its simplicity and efficiency. Again in this section the FDTWEA is used to study the

effect of the electrode wall angle that is the most practical effects due to fabrication processes. In extending the bandwidth of the device, very thick electrodes of thickness ranges from 10-20 μm is used. Such thick electrodes, however, do not assume a perfect 'brick wall' shape. They are more likely to take up a trapezoidal shape as shown in Figure 1. Such geometrical factor cannot be ignored because they certainly have a subtle effect on both the values of Z and n_m. Gopal *et al.*[21] have modelled the effect with their finite element calculation. We shall study the effect of the wall angle with our finite difference model to demonstrate the capability of our numerical model. Similar electrode structures and dimension similar to that reported in [21] have been adopted in our experimental works.

The wall-angle of tilted electrodes significantly affects the effective values of Z and n_m. The effect of the wall angle is less severe for thinner electrodes as we can see from Figure 8 that the differences of the plots for different θ converge as the electrodes become thinner. For thick electrodes, especially those that are greater than 10 μm, the wall angle effect should not be ignored. For example, if we base our design on the assumption of a θ=90° rectangular electrode, then we would use a 20 μm thick electrode for the best velocity match. However if the fabricated electrodes actually assume a trapezoidal shape with θ=80°, we would have overestimated the value of n_m for best velocity matching by about 0.2. This corresponds to almost a 20% loss of the bandwidth that could have been achieved by a mismatch of 0.01 between the microwave index and the optical propagation velocity. Modelled results indicate that an electrode thickness of around 14μm can be used to achieve maximum bandwidth. Based on the assumption of an 82° electrode wall angle and an electrode of a thickness of 15 μm[21]. We have thus shown another potential application of our finite difference numerical modelling scheme in offering much analytical capability that would be

beyond most analytical techniques such as the Green function method[4.5], spectral domain analysis[9], conformal mapping[1], or method of image[3,15]. Undoubtedly, a greater analytical capability would certainly imply a better design in travelling wave electrodes for integrated optical modulators.

3.4   Modulator implementation

Optical waveguides are fabricated by Ti:diffusion of about 500 A^o thick under a diffusion time of 7 hours. SiO2 layer is then sputtered with thickness variable from 0.6 to 2.0 μm. Electrodes are formed by two main stages. A 200 A^o chrome layer is first deposited and the electrode pattern is then photolithographically created. A 1000A^o thick Au layer is then deposited on top of the Cr temporary electrode pattern. The gold layer is then etched to the pattern of the eletrode structures. Electroplating of thick Au pattern is then conducted. The thickness of electroplated Au can reach 7 to 10 μm with a wall angle of about 12 to 20 degrees without shorting the electrodes. Note that prior to the fabrication of the electrode, optical channel waveguides are tested using the straight optical channels pattern next to the Mach-Zehnder structures in order to determine the important parameters of the electrodes as designed and simulated. Microwave coupling and mounting are packaged and fibre pigtails are then performed.

The inserion loss S_{21} of the fabricated electrodes are simulated and measured and are consistent as predicted and shown in Figure 9. Figure 10 shows the measured RF insertions loss with the upper curve showing the calibrated S_{21} of the microwave set up and the lower curve showing the results for the case when the RF electrodes are included in the measured system. Several modulators have been fabricated. The obtained results indicate that the electrical and optical bandwidths reach a

consistent range of about 26 GHz to 30 GHz. Optical measurement of the packaged modulators have also been obtained and the optical transfer bandwidths are compatible with those obtained in the electrical domain. This concludes that the optical loss is minimum and a good velocity matching between the optical waves and the travelling microwaves. Experimental results will be described in details.

4   CONCLUDING REMARKS

A numerical model has been modulated to conduct analytical, effective and efficient modelling of electrode performance and electro-optic interaction for optical modulation of guided lightwaves via the interferometric structures. The anisotropic Laplace equation (1) solved by using the finite difference techniques leads an accurate and efficient model of the microwave properties of various electrode structures. A non-uniform grid allocation scheme is minimise the demand on memory usage. The numerical FDTWEA has been shown to be efficient without jeopardising the accuracy of the calculated results. Calculated values of the characteristic impedance Z and the microwave effective index n_m obtained by this method are consistent with those reported in published articles over the last two decades. The comparison of FDTWEA' calculations with the finite element method[19, 20] has promised a great consistency between the two computation techniques and hence the effectiveness of the finite difference presented in this paper, in computing resources and potentials in its applications in complex electrode structures of optical modulators.

The FDTWEA has been incorporated in interferometric modulators in estimating the interaction overlap integral, Γ. The calculation of Γ is useful to ensure that a device with a low half wave voltage, V_π and hence lower power driven optical modulator can be realised. Further we have

shown the efficiency of the FDTWEA in analysing a complex electrode structure, the shielded phase-velocity matched electrode structure. It is shown that FDTWEA can be used effectively in analysing the electrode in practical modulators. We also model the effects of the trapezoidal shape electrode with the wall angle θ, as assumed by most thick electrode (>10 μm) fabricated by present electroplating technique. This effect could not be easily modelled by most analytical techniques such as the conformal mapping method of image, Green function method or spectral domain analysis. The subtle effect of the wall angle, however, has been modelled without difficulty by FDTWEA.

Experimental results have been obtained for optical MZ modulators with an electrical/optical bandwidth reaching 26 to 30 GHz with an electrode thickness of more than 5 μm and an estimate wall angle of about 12 degrees. This indicates the accuracy of the electrode modelling and the simple fabrication techniques of the electrodes and optical waveguide structures.

REFERENCES

1. O.G.Ramer, "Integrated optic electrooptic modulator electrode analysis", *IEEE J. Quant. Elect.*, **QE-18**, pp.386-392, 1982.

2. D. Marcuse, "Optimal electrode design for integrated optics modulators", *IEEE J. Quant. Elect.*, **QE-18**, pp.393-398, 1982.

3. C. Sabatier and E. Caquot, "Influence of a dielectric buffer layer on the field distribution in an electrooptic guided wave device", *IEEE J. Quant. Elect.*, **QE-22**, pp. 32-37, 1986

4. H.Chung, W.S.C. Chang, and E.L. Adler, "Modelling and optimisation of travelling-Wave LiNbO$_3$ Interferometric modulators", *IEEE J. Quant. Electron.*, **QE-27**, pp.608-617, 1991.

5. H. Chung, W.S.C. Chang, and G.E. Betts, "Microwave properties of travelling-wave electrode in LiNbO$_3$ electrooptic modulators", *IEEE J. Lightw. Tech.*, **11**, pp.1274-1278, 1993.

6. M. Seino, *et al.*, "20 GHz 3 dB-bandwidth Ti:LiNbO$_3$ Mach-Zehnder modulator", Proc. ECOC '90, pp.999-1002, postdeadline paper, 1990.

7. R.A. Becker, "Broadband guided wave electrooptic modulators", *IEEE J. Quant. Elect.,* **QE-20**, pp.723-727, 1984.

8. H. Jin, M. Bélanger and Z. Jakubezyk, "General analysis of electrodes in integrated optics electrooptic devices", *IEEE J. Quant. Elect.*, **27**, pp.243-251, 1991.

9. K. Kawano *et al.*, "A wide-band and low driving power phase modulator employing a Ti:LiNbO$_3$ optical waveguide at 1.5 μm wavelength", *IEEE Photonics Tech. Lett.,* **1,** pp. 33-34, 1989.

10.   T. Kitoh and K. Kawano, "Modelling and design of Ti:LiNbO$_3$ optical modulator electrodes with a buffer layer, Elect. & Comm. Japan, Part 2, **76**, pp.25-34, 1993.

11.   K. Kawano *et al.*, "New travelling -wave electrode Mach-Zehnder optical modulator with 20GHz bandwidth and 4.7V driving voltage at 1.52", *Elect. Lett.*, **25**, pp. 20-21, 1989.

12.   K. Kawano *et al.*, "Design and fabrication of shielded velocity matched Ti:LiNbO$_3$ optical modulator", *Elect. & Comm.Japan*, Part 2, **75**, pp. 9-19, 1992.

13.   see for example (a) Z. Pantic and R. Mittra, "Quasi-TEM analysis of microwave transmission lines by finite element method", *IEEE Trans. Microw. Th. Tech.,* vol. MTT-34, no. 11, Nov. 1986 and (b) M. Hoshiba, T. Tsuji and M. Nisho, "Finite element modelling of broadband travelling wave optical modulator", IEEE Trans. Microw. Th. Tech., **47**, pp. 1627-1633, 1999.

14.   K. Kenji, N. Kazuto, T. Kitoh and H. Miyazawa, "A finite element method (FEM) analysis of a shielded velocity-matched Ti:LiNbO$_3$ op;tical modulator, *IEEE Photonics Tech. Lett.,* **3**, 1991.

15.   W-C. Chuang *et al.*, "A comparison of the performance of LiNbO$_3$ travelling wave phase modulators with various dielectric buffer layers", *J. Opt. Comm,* **14**, pp. 142-148, 1993.

16.   C.M Kim and R. Ramaswamy, "Overlap integral factors in integrated optic modulators and switches", *J. Lightwave Tech.,* **7,** pp.1063-1070, 1989.

17.   E.L. Wooten and W.S.C. Chiang, "Test structures for characterisation of electrooptic waveguide modulators in lithium niobate", *IEEE J. Quant. Elect.,* **29**, pp.161-170, 1993.

18.   N.H. Zhu, Z.Q. Wang, "Comparison of two coplanar waveguide electrodes for Ti:LiNbO$_3$ interferometric modulators", *Opt. Quant. Elect.* **27**, pp.607-615, 1995.

19.   H.E. Green, "The numerical solution of some important transmission-line problems, *IEEE Trans. Microw. Th. Tech.,* **MTT-13**, pp.676-692, 1965.

20.   G.K. Gopalakrishnan *et al.*, "Electrical loss mechanisms in travelling wave LiNbO$_3$ optical modulators", *Elect. Lett.,* **28,** pp. 207-208, 1992.

21.   G.K. Gopalakrishnan *et al.*, "Performance and modelling of broadband LiNbO$_3$ travelling wave optical intensity modulators", *J. Lightw. Tech.,* **12**, pp. 1807-1818, 1994.

22.   S.K. Korotky *et al.*, "Optical intensity modulation to 40GHz using a waveguide electro-optic switch", *App. Phys. Lett.*, **50**, pp.1631-1633, 1987.

23.   C.M Gee *et al.*, "17 GHz bandwidth electro-optic modulator", *App. Phys. Lett.*, **43**, no. 11, 1 Dec. 1983.

24.   W. Charczenko *et al.*, "Characterization and simulation of proton exchanged integrated optical modulators with various dielectric buffer layers", *J. Lightwave Tech.,* **9**, pp.92-100, 1991.

25.   S.Y. Liao, Microwave Circuit Analysis and Amplifier Design, Prentice-Hall International Editions.

26.   K. Atsuki and E. Yamashita, "Transmission line aspects of the design of broad band electrooptic travelling-wave modulators, *IEEE J. Lighwave Tech.,* **LT-5**, pp. 316-319, 1987.

27.   S. Ramo and R.W. Whinery, "Fields and Waves in Communication Electronics", 2nd Edition, John Wiley & Sons, Inc.

28.   D. Hoffman, *Fortran 77: A Structured, Discipline Style*, 2nd Edition, McGraw Hill Book Company.

29.   M. R. Spiegel, *Mathematical Handbook of Formulas and Tables*, Shaum's Outline Series, McGraw hill Book Company.

30.   W. H. Press *et al.*, *Numerical recipes-the art of scientific computing*, Cambridge University Press, pp.240-246.

31.   T. C. Oppe et al., NSPCG user's guide V. 1.0 - a package for solving large sparse linear systems by various iterative methods, Center for Numerical Analysis, University of Texas, Austin., USA

32.   T. Tamir, *Guided-Wave Optoelectronics,* 2nd Edition, Springer Series in Electronics and Photonics 26, Springer-Verlag.

33.   R. Kraehenbuehl and W.K. Burns, "Modeling of broadband travelling wave optical intensity modulator", IEEE Trans. Microw. Th. Tech., **48**, pp.860-864, 2000.

* All correspondences to le.binh@eng.monash.edu.au
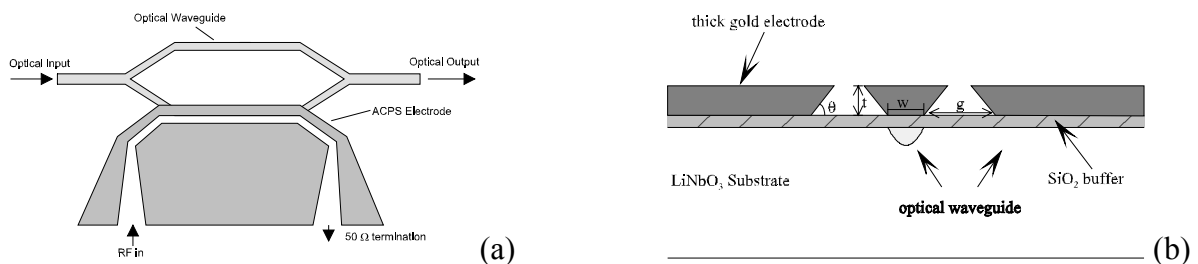
Figure 1 (a) Schematic diagram of the electro-optic interferometric modulator (b) the cross sectional view of wall-angle tilted thick electrodes on optical waveguides.

(a) (b) (c)
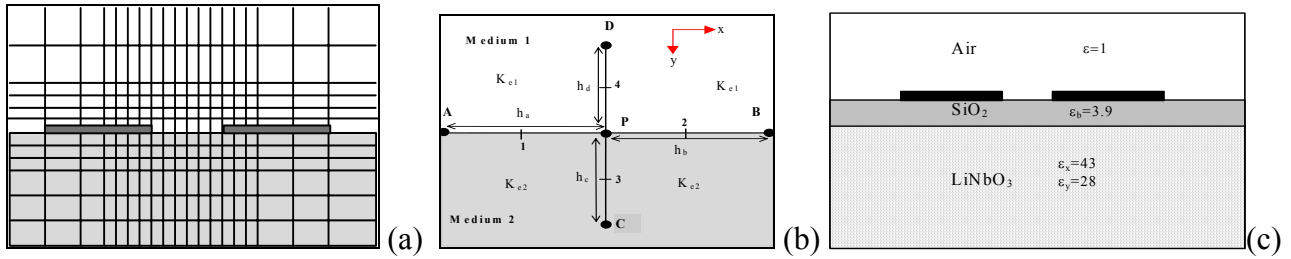
Figure 2 (a) An simple illustration of the non-uniform grid allocation scheme and (b) The grid

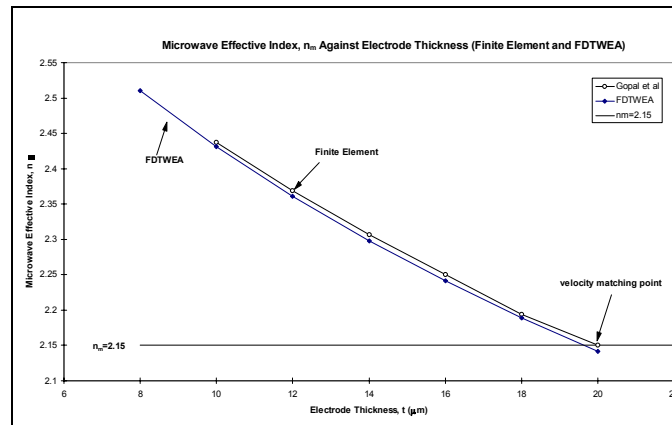points involved in finite differencing (c) dielectric boundary

Figure 4 n_m as calculated by FDTWEA and compared with those obtained by the finite
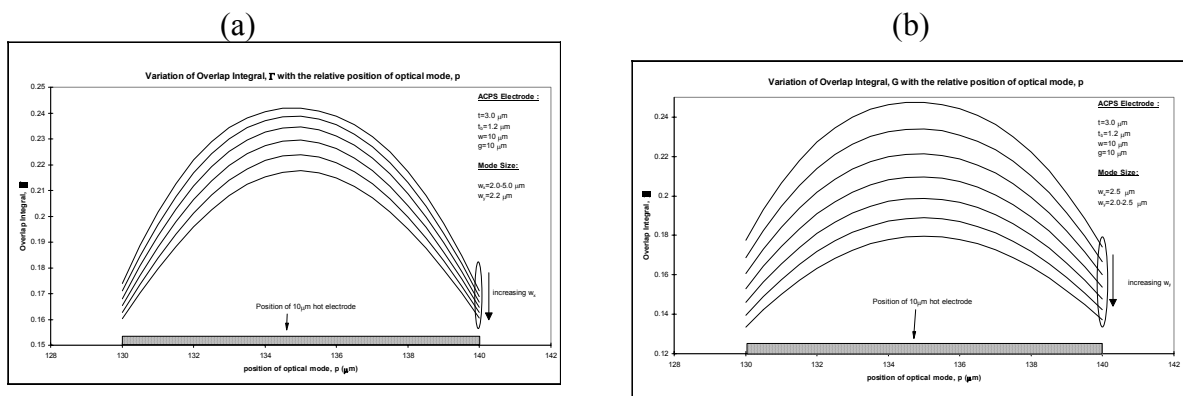
element method

(a)   (b)

Figure 5 Variation of Γ with the peak position of the optical mode shifting from one end of the hot electrode to the other (a) for widening the optical guided mode (b) for increasingly deeper optical mode
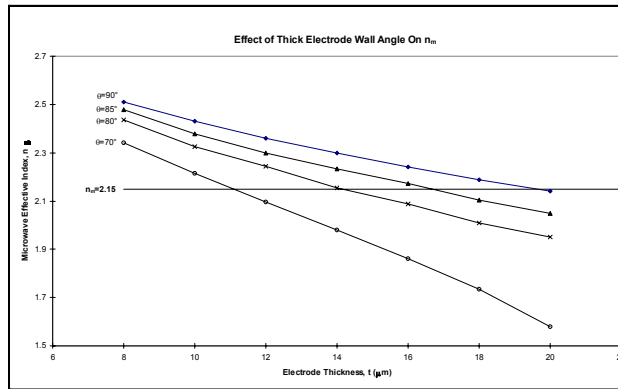
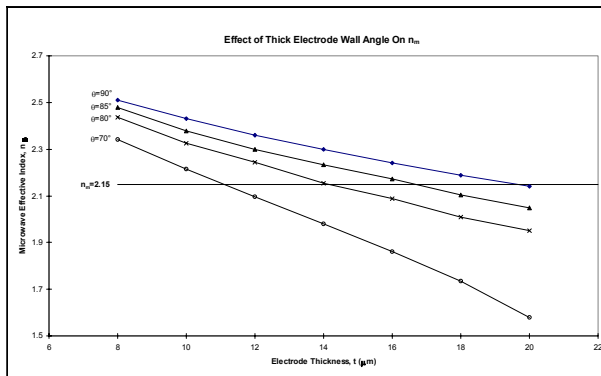Figure 7 Γ as a function of the thickness of SiO$_2$ buffer, t$_b$
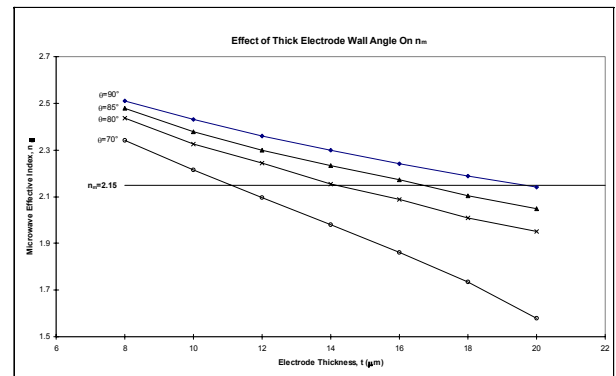
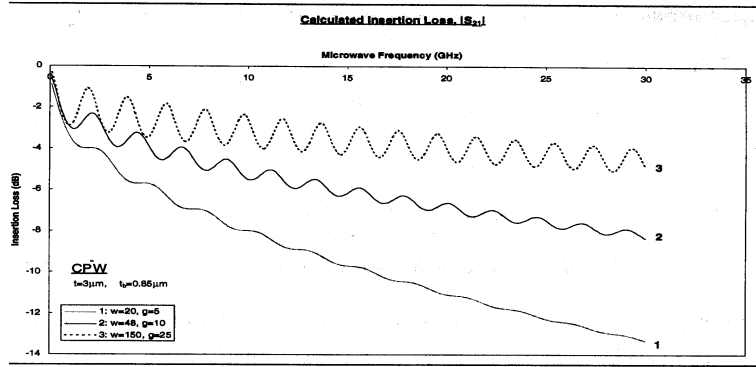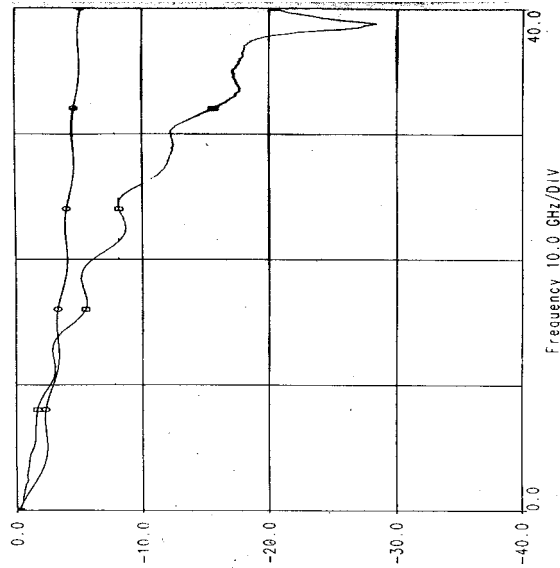*Figure 8   Dependence on n$_m$ and Z on the wall angle of the thick electrode.*

Figure 9 Inserion loss S_{21} of the RF electrode as a function of the microewave frequency

Electrical/optical signal "gain"

Fgure 10 Electrical (S_{21})/Optical response of the implemented interferometric modulator